Exploration of Vitamin B_6-Based Redox-Active Pyridinium Salts towards the Application in Aqueous Organic Flow Batteries

Anton A. Nechaev,[a+] Gabriel Gonzalez,[b+] Prachi Verma,[a] Vsevolod A. Peshkov,[a] Anton Bannykh,[a] Arsalan Hashemi,[c] Jenna Hannonen,[b] Andrea Hamza,[d] Imre Pápai,[d] Kari Laasonen,[c] Pekka Peljo,[b]* Petri M. Pihko[a]*

[+] denotes equal contribution

[a] Department of Chemistry, University of Jyväskylä, P. O. Box 35, Jyväskylä, 40014, Finland

[b] Research Group of Battery Materials and Technologies, Department of Mechanical and Materials Engineering, Faculty of Technology, University of Turku, Turku, 20014, Finland

[c] Department of Chemistry and Material Science, School of Chemical Engineering, Aalto University, Espoo, 02150, Finland

[d] Institute of Organic Chemistry, HUN-REN Research Centre for Natural Sciences, Magyar tudósok körutja 2, Budapest, 1117, Hungary

pekka.peljo@utu.fi, petri.pihko@jyu.fi

Abstract

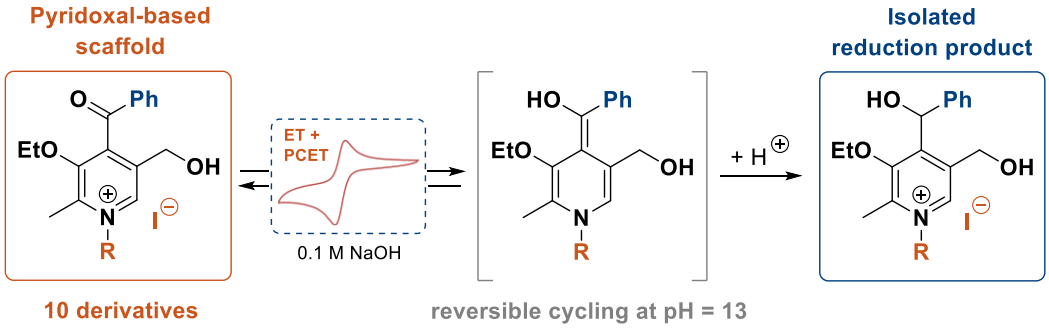

We have examined the utility of pyridoxal hydrochloride, a vitamin B_6 vitamer and a biobased feedstock, as a starting point towards organic redox flow battery materials. Pyridoxal hydrochloride was synthetically converted to a series of diverse vitamin B_6-based redox-active benzoyl pyridinium salts. These compounds were electrochemically characterized through cyclic voltammetry (CV) measurements in neutral and basic aqueous electrolytes (1 M KCl and 0.1 M NaOH). Based on the CV results, which demonstrated reversibility under basic conditions, two of the most promising salts were subjected to laboratory-scale redox flow battery tests involving galvanostatic cycling at 10 mM with 0.1 M NaOH as the supporting electrolyte. These results showed that the battery was charged completely, corresponding to the transfer of two electrons to the electrolyte, but no discharge was observed. Both CV analysis and electrochemical simulations confirmed that the redox wave observed in the experimental voltammograms corresponds to a two-electron process. To explain the irreversibility in the battery tests, we conducted bulk electrolysis with the benzoyl pyridinium salts, affording the corresponding benzylic secondary alcohols. This process involves the transfer of two electrons and two protons to reduce the ketone group to alcohol. Computational studies suggest that the reduction proceeds in three consecutive steps: first electron transfer (ET), then proton-coupled electron transfer (PCET) and finally proton transfer (PT). ^{1}H NMR deuterium exchange studies indicated that the last PT step is not reversible in 0.1 M NaOH, rendering the entire redox process

irreversible. The apparent reversibility observed in CV at the basic media likely arises from the slow rate of the PT step at the timescale of the measurement.

Introduction

In recent years, the amount of electrical energy generated from intermittent renewable sources has been continuously increasing[1]. This boosts the demand for the production of energy storage facilities of medium and large scales. Flow Batteries (FBs) are viewed as one of the most promising technologies for solving this issue[2]. A unique opportunity to tailor the electrode surface area as well as the volume and concentration of a working electrolyte is deemed to be the key for incorporating such batteries to variously sized electrical grids.

Classical and well-developed Vanadium Flow Batteries (VFB) represent a significant part of a commercially implemented batteries of this type[3]. Despite their great stability, the price of raw materials and the toxicity of electrolytes prompt researchers to search for alternative solutions[4]. Accordingly, Organic Flow Batteries (OFB) have been introduced as the next-stage opportunity for large-scale electrical energy storage. Low prices, accessibility, and abundance of organic electroactive materials could make OFB financially more attractive in a long-term perspective. Recently, special attention has been paid to Aqueous Organic Flow Batteries (AOFBs) - water-based, non-flammable, and easily maintained OFBs sub-division[5]. Utilization of aqueous electrolytes offers the safest and cheapest settings for FBs implementation on industrial scale. Anthraquinones[6], TEMPO-derivatives[7], fluorenones[8], flavins[9] are among the most prominent molecules used in aqueous electrolytes that have been developed to date. Despite substantial progress in this area, the search for new cost-effective, safe, and scalable water-soluble redox-active organic molecules for AOFBs continues[10].

Pyridinium salts occupy a significant niche in organic chemistry[11]. Known as redox-active functional group transfer reagents for a variety of chemical transformations[12], it is not surprising that *N*-functionalized pyridinium scaffolds were identified as promising candidates for redox-active materials in RFBs. In particular, promising results have been achieved with bipyridinium-based viologens[13] and diquats[14], benzoyl-substituted pyridinium ions (in both non-aqueous[15] and aqueous[16] media) and pyridinium-carbene hybrids[17].

A realistic redox flow battery material should also be available in sufficient quantities, ideally from natural sources. Among the pyridine-based biobased molecules, vitamin B_6 was viewed as a highly promising candidate. Vitamin B_6 comprises a series of six pyridine-based chemically related derivatives, so-called "vitamers" that are interconvertible in living systems, with the pyridoxal 5'-phosphate being an active form (Figure 1)[18]. All B_6 vitamers are water soluble, available via fermentation[19], and likely to possess high biodegradability. All these properties are highly advantageous for prospective AOFB molecules. Furthermore, the presence of pre-installed functional groups renders B_6 vitamers excellent candidates for a broad synthetic exploration[20,21,22,23].

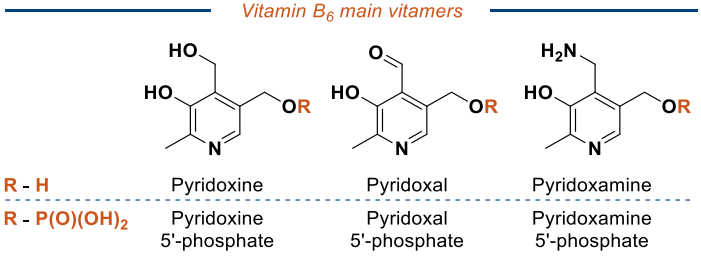

Figure 1. Vitamin B_6 vitamers

In our previous study, we described the development of a computational protocol that combines semiempirical and DFT quantum chemical methods to predict the redox potentials as well as the stability of reduced species of perspective vitamin B_6-based aqueous electrolytes[24]. The outlined framework revealed the set of vitamin B_6 derivatives with the predicted redox potentials falling within the electrochemical stability window of water[25]. Herein we report a general synthetic platform to access a wide range of water-soluble *N*-alkylated benzoyl pyridinium salts based on vitamin B_6 as well as the experimental assessment of their electrochemical behaviour and performance in flow batteries.

Synthetic modification of the vitamin B_6 core

We have chosen commercially available pyridoxal hydrochloride, the oxidized form of vitamin B_6 as a starting point for synthetic exploration. The proposed outline is shown in Scheme 1 and involves the nucleophilic Grignard addition to the aldehyde group followed by the oxidation to introduce a benzoyl pyridine motif. Phenolic and benzylic hydroxy groups that would likely require protection during the implementation of the above sequence can later be used for generating more derivatives via functional group interconversion. In the final stage, the alkylation of pyridine nitrogen enables formation of pyridinium salts.

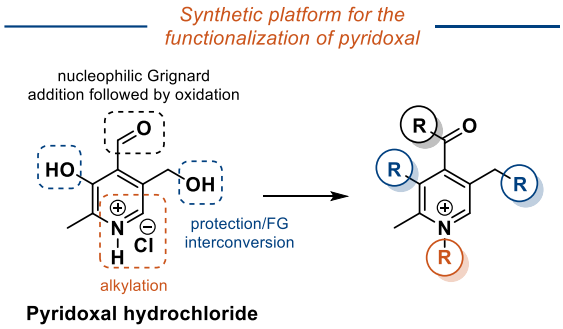

Scheme 1. Outline for the synthetic elaboration of pyridoxal hydrochloride

The initial attempts to functionalize carbonyl group with phenyl magnesium chloride failed likely due to the insolubility of pyridoxal in organic solvents. Accordingly, installing lipophilic silyl groups has been proposed as a convenient solution to increase the solubility of pyridoxal and to avoid an interference of unprotected OH groups with the Grignard reagent. Treating pyridoxal hydrochloride with *tert*-butyldimethylsilyl chloride in the presence of DABCO in acetonitrile led to the formation of bis-silylalted pyridoxal ether **1** in 97% of yield (Scheme 2). Subsequent functionalization of **1** with phenyl magnesium chloride gave a rise to secondary alcohol **2** in 78% of yield. Oxidation of **2** with Dess–Martin periodinane in dichloromethane led to the formation of benzoyl pyridine **3** in 55% of yield. *N*-alkylation of pyridoxoketone **3** was accomplished using appropriate iodoalkanes in DCM at 50°C and resulted in a mixture of mono- and bis-silylated benzoyl pyridinium species **4** and **4'**, respectively. Treating crude mixture **4**/**4'** with ammonium fluoride in methanol at room temperature provided zwitter-ionic pyridinium derivatives **5a** and **5b** in good yields with the structure of **5b** being confirmed by a single crystal X-Ray diffraction (XRD) analysis (CCDC 2325623).

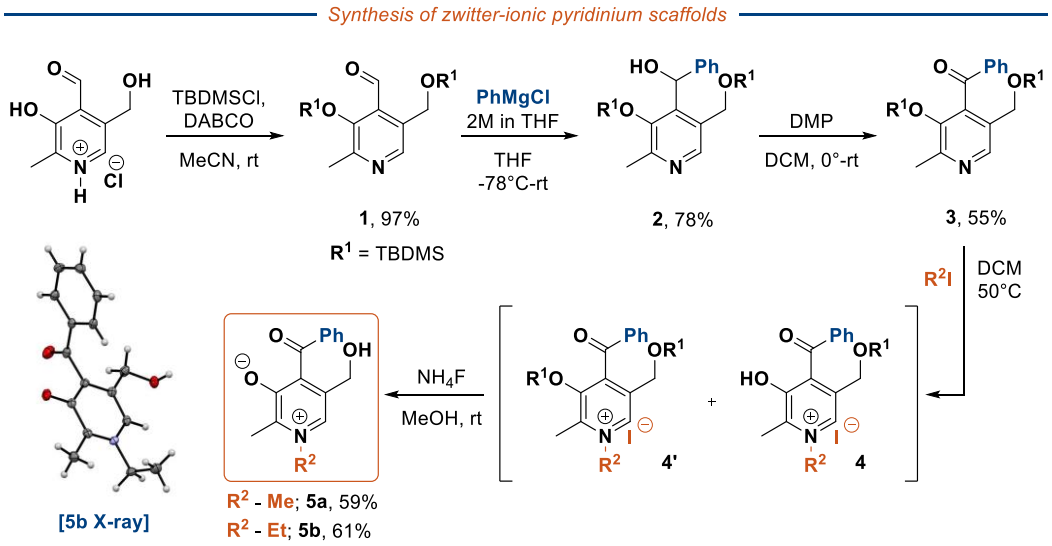

Scheme 2. Synthesis of zwitterionic pyridinium derivatives **5a**-**b**

Subsequently, compounds **5a**-**b** were subjected to electrochemical studies, but voltammetry tests showed a non-reversible reduction process at a very negative potential close to water reduction (see electrochemical exploration for details).

Therefore, we devised a new synthetic route that rules out the formation of zwitterionic compounds (Scheme 3). The key idea was to expose the phenolic OH group via partial deprotection of bis-silylated pyridoxal **1** and then block it via *O*-alkylation. To our delight, stirring **1** in acetone/water (v:v = 5:1) mixture led to selective cleavage of one of the TBDMS-groups affording mono-silylated analogue **6** in 92% yield. Subsequent treatment of **6** with ethyl iodide and potassium carbonate in DMF furnished *O*-alkylated aldehyde **7** in 67% yield. Subjecting aldehyde **7** into Grignard addition/DMP oxidation sequence allowed to obtain benzoyl pyridines **9a**-**c** in good overall yields. TBAF-promoted desilylation of **9a**-**b** gave a rise to pyridoxal derivatives **10a**-**b**. Finally, *N*-alkylation of **10a-b** with various iodo- or bromoalkanes delivered a series of *O*,*N*-bis-alkylated pyridinium salts **11a-d** in good yields ranging from 61% to 84%. The structures of representative compounds **11a**-**b** were resolved by single crystal XRD analysis (CCDC 2325625 and 2325624, respectively).

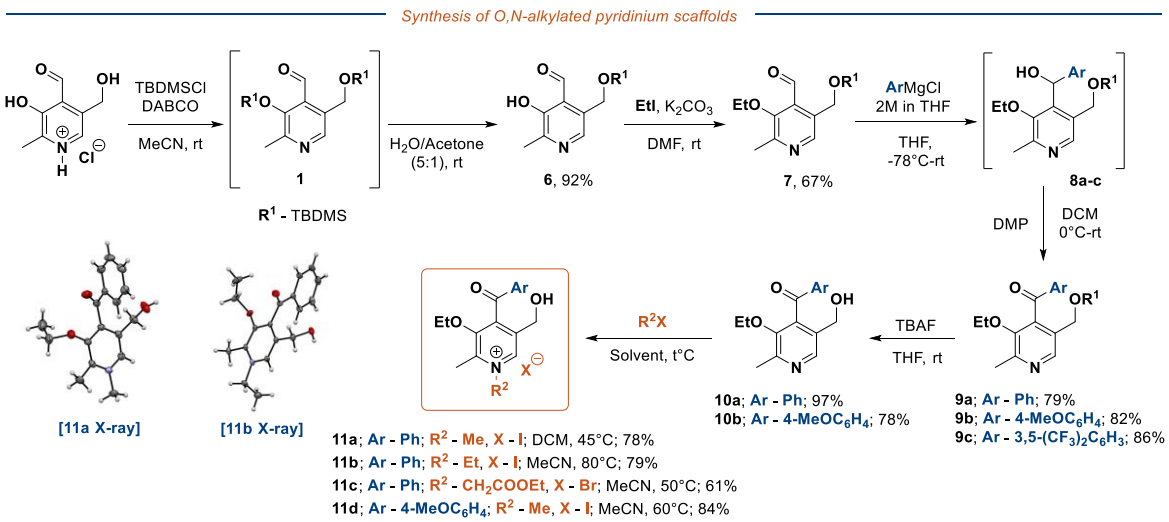

Scheme 3. Synthesis of *O*,*N*-bis-alkylated pyridinium salts **11a**-**d**; for scXRD of **11a** and **11b** iodine atoms are omitted for clarity

Interestingly, desilylation of compound **9c** bearing two electron-withdrawing trifluoromethyl groups on the aryl fragment yielded an interconvertible mixture of benzoyl pyridine **10c** and its hemiacetal **10c'** in 1:10 ratio and 79% overall yield (Scheme 4). Subjecting the obtained mixture to *N*-alkylation with iodomethane led to the exclusive formation of hemiacetal salt **12**. The ease of hemiacetal formation for this substrate can be attributed to the enhanced electrophilicity of the carbonyl group affected by the electron deficiency of the 3,5-bis(trifluoromethyl)phenyl moiety.

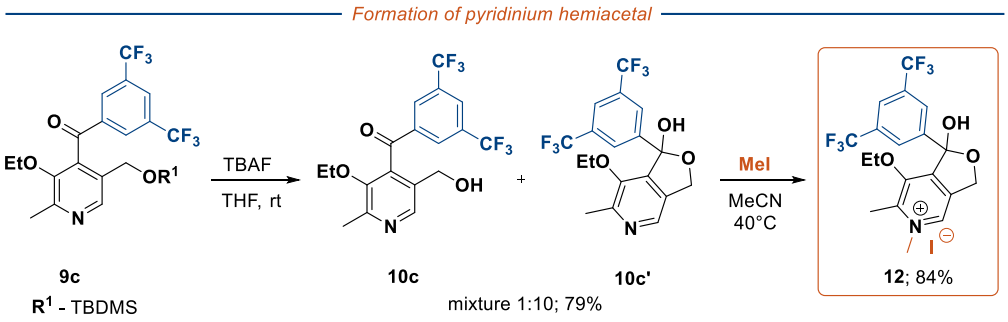

Scheme 4. Formation of hemiacetal salt **12**

The synthetic pathway towards pyridinium salts **11** outlined in Scheme 3 can be slightly altered by reversing the order of two final steps of the sequence that are *N*-alkylation and silyl group removal (Scheme 5). Implementing this approach provided an alternative route to products **11a**-**b** as well as allowed to obtain pyridinium salt **11e** that was unattainable via the original protocol.

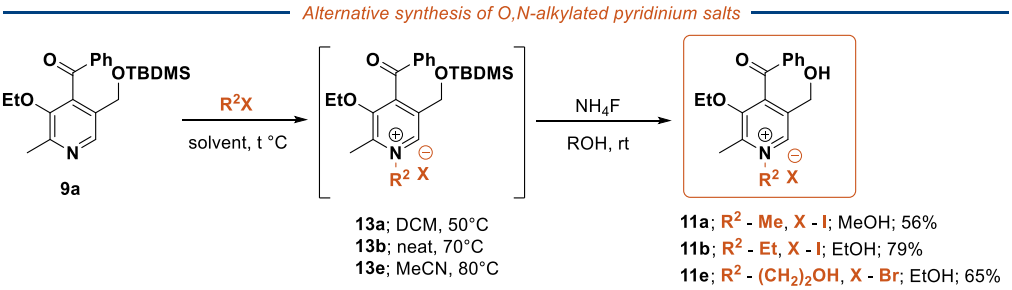

Scheme 5. Alternative alkylation/desilylation sequence for the synthesis of *O*,*N*-bis-alkylated pyridinium salts **11a**-**b**,**e**

Finally, we attempted functionalization of the benzylic hydroxyl group of the pyridoxal core (Scheme 6). Treatment of **10a** with thionyl chloride provided straightforward access to chlorinated pyridoxal derivative **14**. AIBN-promoted reduction with tributyltin hydride produced dechlorinated benzoyl pyridine **15** in 80% yield. *N*-Alkylation of **15** with methyl iodide yielded pyridinium salt **16** lacking benzylic hydroxyl group. An attempt to perform a nucleophilic substitution of chlorine with methoxide produced an inseparable mixture of desired ketone **17** and the corresponding acetal. However, treating the crude mixture thus obtained with 10% aq. HCl in THF delivered the desired ketone **17** in 39% yield along with regenerated **10a** in 52% yield. Subsequent *N*-alkylation of **17** furnished pyridinium salt **18** featuring fully alkylated pyridoxal motif. Next, all the generated pyridinium salts **11**, **12**, **16** and **18** were subjected to electrochemical investigations.

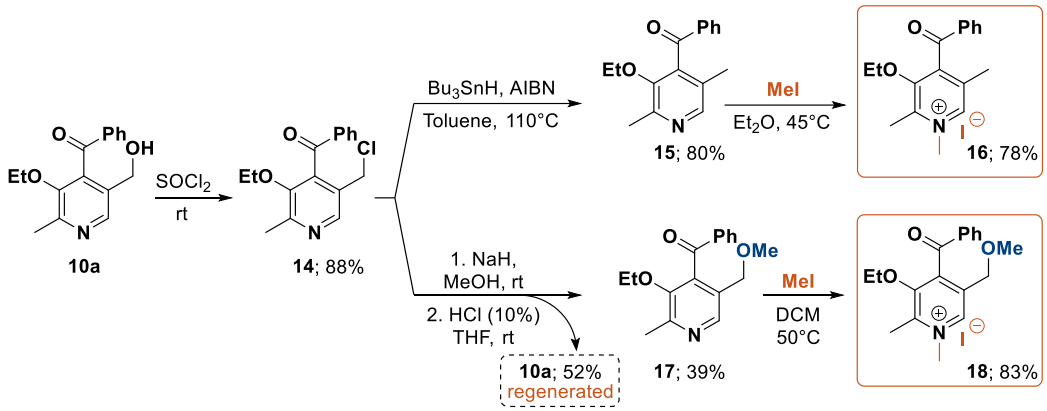

Scheme 6. Synthesis of *O*,*N*- bis-alkylated pyridinium salts **16** and **18** by functional group interconversion

Electrochemical exploration of synthesized pyridoxal derivatives

The initial electrochemical tests consisted of cyclic voltammetry (CV) measurements in aqueous solutions (1 M KCl or 0.1 M NaOH). Previously, benzoyl pyridinium salts have been shown to undergo two one-electron redox processes with the individual redox steps having very close potentials (–0.83 and –0.93 V vs Ag/AgCl)[16]. The first redox process was demonstrated to be reversible; however, the doubly reduced species was unstable in aqueous solutions as it reacts with water. In contrast, voltammograms of the *N*-alkylated benzoyl pyridinium salts studied herein show only one redox event taking place at potentials ranging from –0.86 V to –1.25 V. Details of the CV measurements are presented in the Supporting Information. Table 1 summarizes the voltammetry results by showing the potential of the reduction current peak (reported vs reference Ag/AgCl). The reduction peaks are chosen to assure a proper comparison between the studied compounds as some of them did not show any oxidation peak so the half wave potential cannot be calculated. The experimental reduction potentials observed in 1 M KCl (pH 7) shows a significant agreement with the predicted values from the computational protocol developed by us in the previous study (Figure 2)[24].

Substituent effects on reduction potentials (E_{red}) confirm the established downward trend for the substituents with higher electron donor strength[26]. For example, E_{red} is shifted slightly to more negative values with *N*-ethyl compared to *N*-methyl derivatives (i.e. **5a** vs. **5b,** ΔE_{red} = 10 mV and **11a** vs. **11b** ΔE_{red} = 13 mV, both in 0.1 M NaOH). This shift agrees with the higher electron donating strength of the longer alkyl group. In addition, compounds **11c** and **11e** with electron withdrawing substituents at the end of the *N*-alkyl pendant show a substantial potential shift to higher values compared to **11a** and **11b**. Analogously, compound **11a** bearing hydroxymethyl group in the 5-position of the pyridine core has a more positive potential (E_{red} = –0.952 V) compared to the 5-methyl analogue **16 (**E_{red} = –0.998 V). As expected, moving from the zwitterionic compounds **5a** and **5b** with a deprotonated phenolate oxygen (O^-) to cationic ether derivatives **11a** and **11b**, leads to a significantly more positive reduction potential (for example, for **5a,** E_{red} = –1.242 V *vs*. **11a,** E_{red} = –0.952 V) due to a weaker electron donating strength of ethoxy group compared to the O^- group as well as a higher stability of the reduced species. Introducing methoxy group in the para-position of the benzoyl fragment results in more negative reduction potential (**11e** vs. **11a)** The reduction potential of the hemiacetal derivative **12** measured in 0.1 M NaOH lies in the same range as for benzoyl pyridine derivatives **11** pointing to possible equilibrium between the hemiacetal and keto forms, with the keto form displaying redox activity.

The reduction potential of all compounds measured in both 1 M KCl and 0.1 M NaOH decreases at higher pH, suggesting a proton-coupled electron transfer (PCET) reaction, which is a well-established process in the redox chemistry of quinones[27].

Table 1. Summary of cyclic voltammetry results in 1 M KCl and 0.1 M NaOH. E_{red} corresponds to the potential of the reduction peak against reference Ag/AgCl. I_{ox}/I_{red} is the ratio between the oxidation and reduction peak currents.

Compound	1 M KCl		0.1 M NaOH	
	E_{red} / V	I_{ox}/I_{red}	E_{red} / V	I_{ox}/I_{red}
5a	-[a]	-[a]	-1.242	0[b]
5b	-1.150	0[b]	-1.252	0[b]
11a	-0.802	0[b]	-0.952	0.92
11b	-[c]	-[c]	-0.965	0.91
11c	-0.671	0.22	-0.881	0.65
11d	-0.937	0.29	-0.982	0.92
11e	-0.729	0[b]	-0.866	0.85
12	-[c]	-[c]	-0.950	0.99
16	-0.934	0.21	-0.998	0.37
18	-0.881	0.78	-0.948	0.67

[a] The exact position of reduction current peak cannot be determined.

[b] The value is zero since no oxidation process is present.

[c] Cyclic voltammetry was not performed.

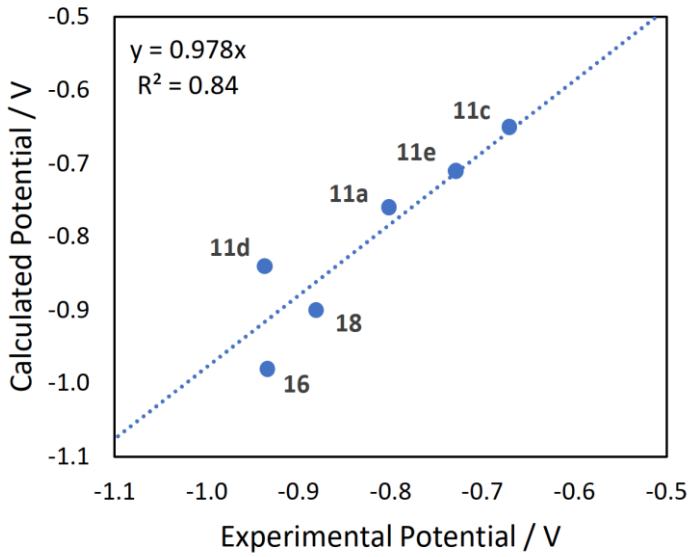

Figure 2. Comparison of the computational and experimental reduction peak potentials of the molecules tested in KCl 1 M (pH 7).

Apart from the potential of the reduction peak (vs reference Ag/AgCl), the ratio between the peak currents (oxidation/reduction) is also reported (see I_{ox}/I_{red} in Table 1). The latter is an indication of the reversibility of the system: the closer this value is to 1, the more reversible the system is. The results presented in Table 1 show that none of the molecules is reversible at neutral pH. The compound **18** shows the highest ratio between the peak currents in that media suggesting quite reversible process. However, the voltammogram exhibits a high sharp oxidation peak that indicates an adsorption of the

reduced species on the working electrode followed by a stripping step during oxidation[28]. The increment of the oxidation current and peak separation at faster scan rates confirms that a weak adsorption process is occurring. That leads to a higher oxidation peak and higher current ratio; however, the process still looks poorly reversible as the current reduces significantly after multiple scans. Most of the tested compounds were found to possess a higher reversibility when tested at basic pH. The best results in 0.1 M NaOH (pH 13) were obtained for compounds **11a**, **11b**, **11d** and **12**. The latter is characterized by the highest current ratio but a very low solubility, even lower than the studied concentration of 1 mM. The compounds **16** and **18** also show low solubility not exceeding 1 mM concentration and thus we did not consider them for further studies.

Next, we investigated the stability of compounds **11a** and **11d** in a laboratory-scale redox flow battery. The studies consisted of galvanostatic cycling using a low concentration (5-10 mM) of the redox material in 0.1 M NaOH as the supporting electrolyte. The experiments were performed in a nitrogen filled glove box at room temperature. A more detailed description of the battery study is provided in the Supporting Information. The results obtained for both materials were similar: the battery was charged completely by the amount corresponding to two electrons, however just a small fraction was discharged back already in the first cycle (less than 1%). These results indicate that the system undergoes a two-electron redox process and that the fully reduced form cannot be oxidized back in the studied aqueous conditions.

Additionally, we studied the redox process via CV analysis and electrochemical simulations. Pyridoxal derivative **11a** was selected as a model compound for these studies because of its high solubility and reversibility. Figure 4 presents the cyclic voltammograms at different scan rates of 1 mM of the active material in 0.1 M NaOH showing one high reversible redox event at –0.932 V, which differs from the two one-electron redox processes of previously studied benzoyl pyridinium salts[15]. Both the peak separation and the Randles-Ševčík equation analysis, presented in detail in the Supporting Information, suggest a two-electron redox process. We further studied and confirmed this via electrochemical simulations. First, we determined the diffusion coefficient using diffusion ordered spectroscopy (DOSY) NMR measurements and then calculated the number of electrons transferred with a model developed in COMSOL Multiphysics software (for details, see the Supporting Information). The simulations confirm that the redox process shown in the experimental voltammogram corresponds to a two-electron process (Figure 5).

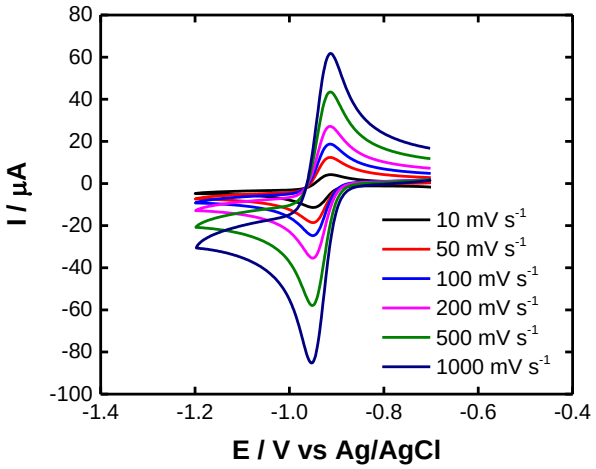

Figure 4. Cyclic voltammograms of 1 mM of compound **11a** at different scan rates in 0.1 M NaOH. Potentials reported against reference Ag/AgCl.

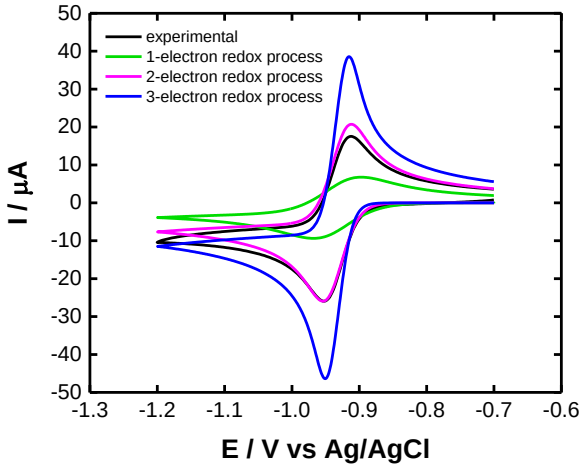

Figure 5. Experimental and simulated cyclic voltammograms of 1 mM of compound **11a** at 100 mV s^{-1} scan rate in 0.1 M NaOH supporting electrolyte. The simulated curves correspond to 1, 2 and 3 electron redox processes. Potentials reported against reference Ag/AgCl.

Electrochemical reduction of pyridoxal-based pyridinium salts

To gain more insight into electrochemical behavior of the synthesized *N*-alkylated benzoyl pyridinium salts, we identified and characterized the products of electrochemical reduction of representative compounds **11a**, **16** and **18**. Conducting bulk electrolysis in an H-cell at constant potential –1.00 V in 1 M potassium chloride (phosphate buffer of pH = 8) yielded corresponding *N*-alkylated pyridoxine analogues **19a**-**c** (Scheme 7). Upon completion of the reduction, alcohols **19a**-**b** could be obtained in a pure form and fully characterized, while **19c** was found to undergo partial oxidation back to **18** under the ambient conditions. Using 0.1 M sodium hydroxide (pH = 13) as the reaction media for bulk electrolysis delivered the same reduction products **19a**-**c**, but the purity of the obtained samples was much lower compared to the reactions in 1 M potassium chloride. As expected on the basis of the electrochemical data (see above), two-electron reduction products **19a-c** were obtained in the bulk electrolysis.

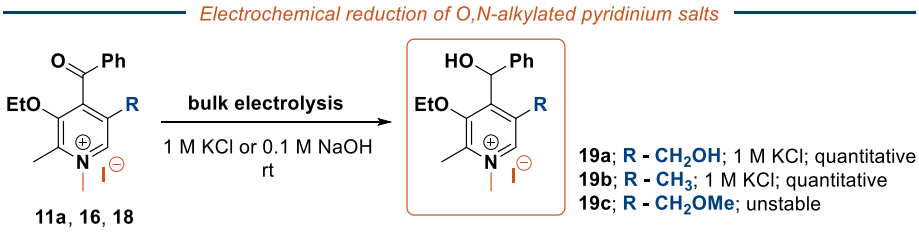

Scheme 7. Electrochemical reduction of **11a**, **16**, **18**

Alcohol **19a** was also synthesized separately in order to provide an independent verification for the structural assignment (Scheme 8). The cyclic voltammogram of the 19a (both 1 M KCl and 0.1 M NaOH), presented in the Supporting information, did not show any reduction nor oxidation peak in the potential window of water, pointing at the electrochemical inactivity of this species.

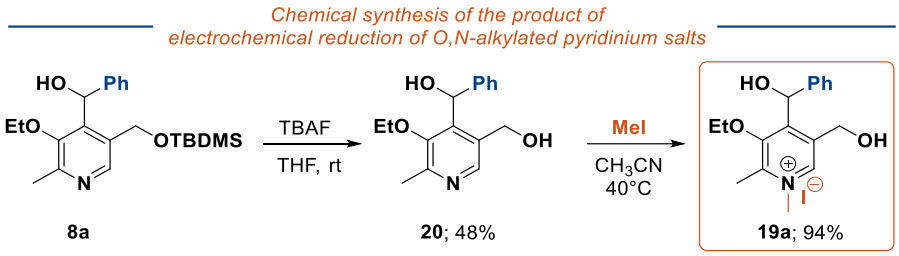

Scheme 8. Synthesis of *N*-alkylated pyridoxine analogue **19a**

Rationale for non-reversibility of the process

Since a two-electron redox cycle would be potentially highly useful for energy storage, we performed a computational study to assess the thermodynamic parameters of electrochemical reduction of **11a** into **19a** in both neutral (pH = 7) and basic (pH = 13) media (Scheme 9). Based on the obtained results, it can be concluded that the initial step of the entire process is the electron transfer (ET) yielding dihydropyridine radical **A**. The computed reduction potential is –0.472 V vs SHE or –0.669 V vs Ag/AgCl. An alternative pathway via radical **B** involving proton-coupled electron transfer (PCET) instead of ET would require achieving substantially more negative potential. The second reduction is likely to occur via a PCET process, yielding enol **C** from dihydropyridine radical **A**. At neutral pH, the reduction potential of this process is –0.533 V vs SHE or –0.730 V vs Ag/AgCl. Alternative pathways involving ET to intermediate **D** or proton transfer (PT) to intermediate **B** would require either more negative potential or more acidic environment, respectively. The computed ET potential for first reduction and PCET potential for second reduction have rather close values suggesting that these processes might occur simultaneously, which agrees well with experimental evidence. Computational data suggests that two processes might be separated at more basic pH through the shift of PCET potential to a more negative value. This, however, is not observed experimentally in cyclic voltammetry studies though the overall two electron reduction potential does shift to a more negative region. Finally, proton transfer (PT) of enol intermediate **C** produces *N*-alkylated pyridoxine **19a**.

The last PT step is likely to be irreversible, which explains the absence of oxidation current peak at neutral pH in the CV curve. At pH 13, the proton transfer is slower so that **11a** can be reduced to intermediate **C** and then oxidized back in the near electrode region during the CV measurements. However, in the laboratory scale battery experiments, protonation of **C** cannot be suppressed and thus the reversibility cannot be achieved as stable product **19a** is formed. To verify this assumption, we assembled a last flow battery using compound **11a** in a more basic electrolyte, 2 M NaOH, which was expected to slow down the PT step. In this case, a much higher amount of the reduced species was oxidized back in the first cycle (8%) and the battery was shortly cycled for five cycles before losing the rest of the capacity. This observation underlines the important role of the protonation on the stability of the doubly reduced species **C**.

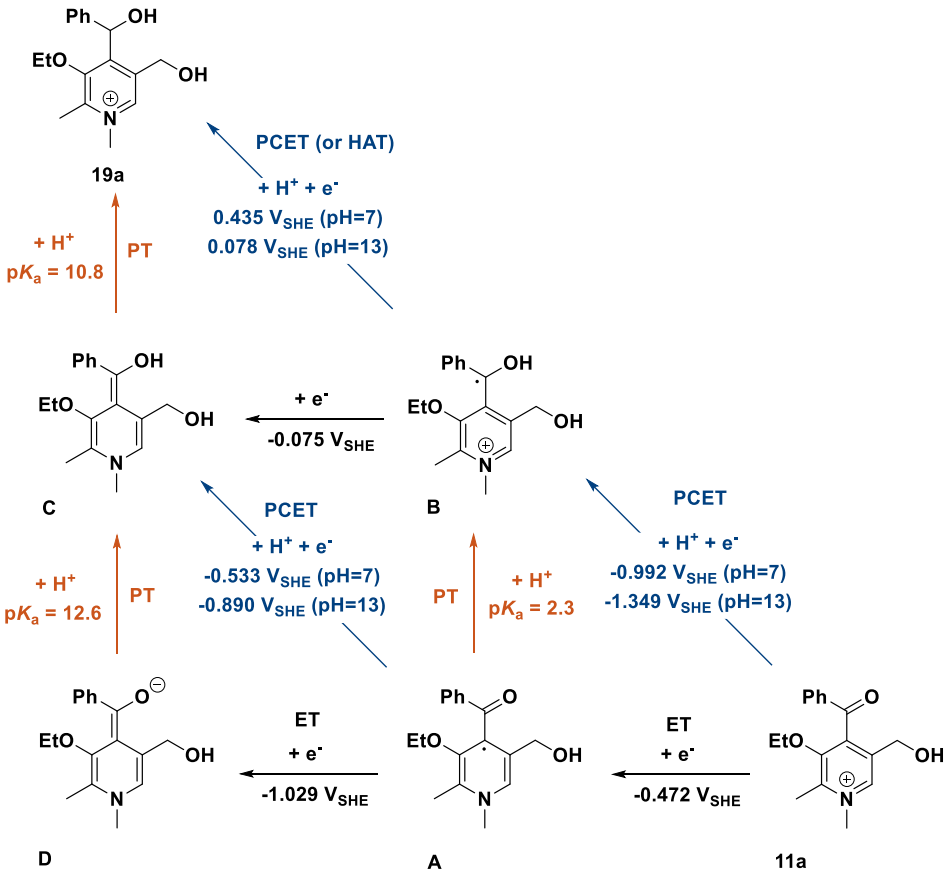

$11a + e^- \rightarrow A$; $E_{red} = -0.472\ V_{SHE} = -0.669\ V_{Ag/AgCl}$
$A + H^+ + e^- \rightarrow D$; $E_{red} = -0.533\ V_{SHE} = -0.730\ V_{Ag/AgCl}$ (pH=7); $E_{red} = -0.890\ V_{SHE} = -1.187\ V_{Ag/AgCl}$ (pH=13)

Scheme 9. Computational square representation for the reduction of compound **11a** (for details, see the Supporting Information). The horizontal direction indicates a reduction reaction through an ET. The vertical direction indicates protonation reactions through a PT reaction. The diagonal direction indicates a reduction reaction through PCET (or hydrogen atom transfer, HAT). The reduction potentials for the PCET steps at the specific pH of 7 and 13 are computed using the Nernst equation.

According to computed p*K*a values, **19a** has four weakly acidic sites with almost equal thermodynamic favourability for deprotonation including the two OH groups and two benzylic C-H groups (Scheme 10a). Experimentally, only the OH protons (sites 2 and 4) are rapidly exchanged with deuterons at neutral pH in D_2O (Scheme 10b). In 0.1 M NaOD in D_2O, slow H/D exchange is observed at the benzylic 2-methyl group (site 1). Even prolonged reaction times did not lead to H/D exchange at site 3, the second benzylic C-H. The electrochemical oxidation of benzylic alcohols is known to be challenging[8,29] since it requires a kinetically slow C-H deprotonation or hydrogen atom transfer / PCET step[30]. Thus, once the two-electron reduction product **19a** is formed, it cannot be deprotonated into the intermediate **C** due to either thermodynamic or kinetic[31] reasons and therefore the subsequent oxidation back into the ketone **11a** cannot be realized.

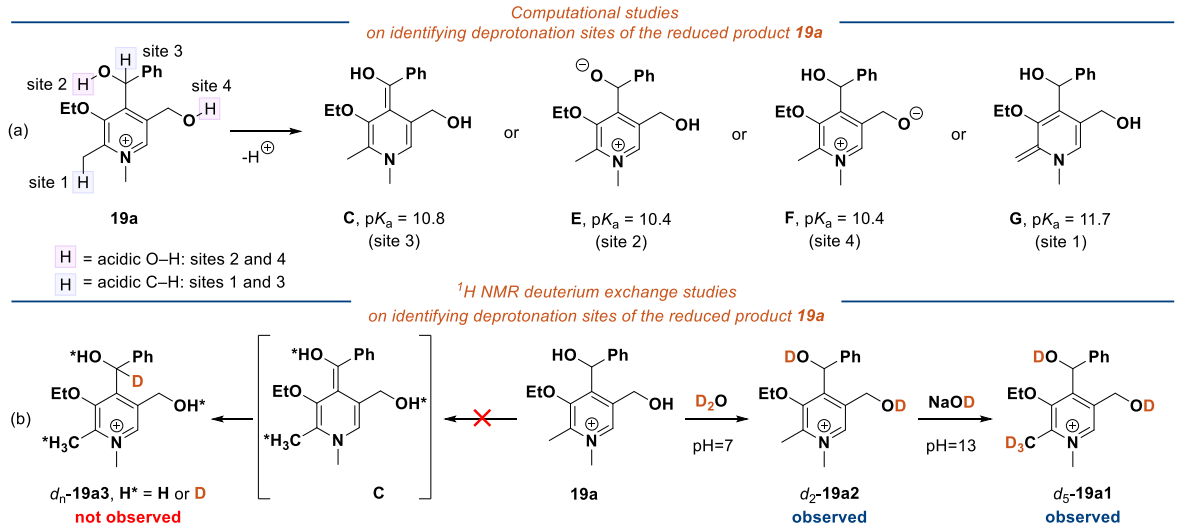

Scheme 10. Studies on identifying deprotonation sites of the reduced product **19a**

Although the computationally predicted reduction potentials for the vitamin B_6-based anolytes were found to be quite reliable, the prediction of irreversibility of the reduction processes in anolyte design, especially in aqueous media, is more challenging. In this study, even candidates that appeared to give a reversible redox cycle in CV tests, such as **11a**, turned out to exhibit irreversible 2-electron-2 proton reduction of the ketone to the benzylic alcohol under laboratory-scale electrolysis tests. In recent molecular designs involving pyridinium-based anolytes, the ketone group has been replaced by other functionalities, such as malononitriles[32] or aryl groups[33] These designs, however, are generally suited for organic solvents instead of aqueous solutions.

Conclusions

In summary, we have outlined the synthetic framework for accessing diverse vitamin B_6-based redox-active benzoyl pyridinium salts starting from the readily available pyridoxal hydrochloride. Altering the structure and electronic properties of the pyridoxal core allowed identifying compounds that showed promise in cyclic voltammetry in basic aqueous media. However, the results obtained with the laboratory-scale RFB were negative. Consequently, we have focused on understanding the electrochemical behaviour of these pyridoxal-based scaffolds. In particular, using CV analysis and electrochemical simulations we have shown that the redox wave observed in the experimental voltammograms of our compounds corresponds to a two-electron process. By performing bulk electrolysis of several representative compounds we were able to isolate and characterize the reduction products incorporating the secondary alcohol moiety resulting from 2-electron reduction of the ketone carbonyl. Based on the experimental evidence and computational data, the overall transformation follows a ET/PCET/PT sequence, with the first two steps occurring at the same reduction potential and the final protonation step being irreversible. Overall, the integrated approach, including bulk electrochemistry tests, turned out to be a highly reliable workflow for assessing the viability of compounds for electrochemical applications in aqueous solutions. Furthermore, the results obtained by us could be useful for designing next generation redox active pyridoxal/pyridinium ketone derivatives suitable for RFB technology. In particular, additional efforts can be directed to introducing scaffold changes that can either suppress the late-stage protonation or facilitate the separation of ET and PCET towards reversible cycling at the potential of first electron transfer.

Acknowledgments

This project has received funding from the European Union's Horizon2020 Research and Innovation programme under grant agreement No 875565 (Project CompBat). Support from Research Council of Finland (projects 322899, 348328 (to P.M.P.) and 346895 (to A. N.) as well as project DIGIPOWER (Technology Industries of Finland Centennial Foundation and Jane & Aatos Erkko Foundation) is also acknowledged. A.B. thanks the Chemistry Department of University of Jyväskylä for funding, Prof. Kari Rissanen for training in crystallography and assistance in measurement of the structures **5b** and **11a**. The organizing committee of Zurich Summer School of Crystallography is thanked for assistance in measuring and solving the structure **11b** (in particular Dr. Michael D. Wörle, Dr. Nils Trapp and Dr. Farzaneh Fadaei-Tirani). PP gratefully acknowledges the Academy Research Fellow funding (grant no. 315739, 343791, 320071 and 343794) and BioFlow project (grant no. 343493) from Academy of Finland, and European Research Council through a Starting grant (agreement no. 950038).

References

[1] a) M. Z. Jacobson, M. A. Delucchi, Z. A. F. Bauer, S. C. Goodman, W. E. Chapman, M. A. Cameron, C. Bozonnat, L. Chobadi, H. A. Clonts, P. Enevoldsen, J. R. Erwin, S. N. Fobi, O. K. Goldstrom, E. M. Hennessy, J. Liu, J. Lo, C. B. Meyer, S. B. Morris, K. R. Moy, P. L. O'Neill, I. Petkov, S. Redfern, R. Schucker, M. A. Sontag, J. Wang, E. Weiner, A. S. Yachanin, *Joule* **2017**, *1*, 108-121; b) P. Das, J. Mathur, R. Bhakar, A. Kanudia, *Energy Strategy Rev.* **2018**, *22*, 1-15.

[2] G. L. Soloveichik, *Chem. Rev.* **2015**, *115*, 11533-11558.

[3] K. Lourenssen, J. Williams, F. Ahmadpour, R. Clemmer, S. Tasnim, *J. Energy Storage* **2019**, *25*, 100844.

[4] D. Larcher, J.-M. Tarascon, *Nat. Chem.* **2015**, *7*, 19.

[5] a) Y. Liu, Q. Chen, P. Sun, Y. Li, Z. Yang, T. Xu, *Mater. Today Energy* **2021**, *20*, 100634; b) Z. Li, T. Jiang, M. Ali, C. Wu, W. Chen, *Energy Stor. Mater.* **2022**, *50*, 105-138.

[6] a) B. Huskinson, M. P. Marshak, C. Suh, S. Er, M. R. Gerhardt, C. J. Galvin, X. Chen, A. Aspuru-Guzik, R. G. Gordon, M. J. Aziz, *Nature* **2014**, *505*, 195-198; b) B. Hu, J. Luo, M. Hu, B. Yuan, T. L. Liu, *Angew. Chem. Int. Ed.* **2019**, *58*, 16629-16636; c) E. F. Kerr, Z. Tang, T. Y. George, S. Jin, E. M. Fell, K. Amini, Y. Jing, M. Wu, R. G. Gordon, M. J. Aziz, *ACS Energy Lett.* **2022**, *8*, 600-607.

[7] a) Y. Liu, M.-A. Goulet, L. Tong, Y. Liu, Y. Ji, L. Wu, R. G. Gordon, M. J. Aziz, Z. Yang, T. Xu, *Chem* **2019**, *5,* 1861-1870; b) B. Hu, M. Hu, J. Luo, T. L. Liu, *Adv. Energy Mater.* **2021**, *12*, 2102577; c) M. Pan, L. Gao, J. Liang, P. Zhang, S. Lu, Y. Lu, J. Ma, Z. Jin, *Adv. Energy Mater.* **2022**, *12*, 2103478.

[8] R. Feng, X. Zhang, V. Murugesan, A. Hollas, Y. Chen, Y. Shao, E. Walter, N. P. N. Wellala, L. Yan, K. M. Rosso, W. Wang, *Science* **2021**, *372*, 836-840.

[9] A. Orita, M. G. Verde, M. Sakai, Y. S. Meng, *Nat. Commun.* **2016**, *7*, 13230.

[10] A. Ramar, F.-M. Wang, R. Foeng, R. Hsing, *J. Power Sources* **2023**, *558*, 232611.

[11] S. Sowmiah, J. M. S. S. Esperança, L. P. N. Rebelo, C. A. M. Afonso, *Org. Chem. Front.* **2018**, *5*, 453-493.

[12] S. L. Rössler, B. J. Jelier, E. Magnier, G. Dagousset, E. M. Carreira, A. Togni, *Angew. Chem. Int. Ed.* **2020**, *59*, 9264-9280.

[13] a) T. Liu, X. Wei, Z. Nie, V. Sprenkle, W. Wang, *Adv. Energy Mater.* **2015**, *6*, 1501449; b) S. Jin, E. M. Fell, L. Vina-Lopez, Y. Jing, P. W. Michalak, R. G. Gordon, M. J. Aziz, *Adv. Energy Mater.* **2020**, *10*, 2000100; c) M. Hu, W. Wu, J. Luo, T. L. Liu, *Adv. Energy Mater.* **2022**, *12*, 2202085.

[14] J. Huang, Z. Yang, V. Murugesan, E. Walter, A. Hollas, B. Pan, R. S. Assary, I. A. Shkrob, X. Wei, Z. Zhang, *ACS Energy Lett.* **2018**, *3*, 2533-2538.

[15] a) N. Leventis, I.A. Elder, X. Gao, E. W. Bohannan, C. Sotiriou-Leventis, A. M. Rawashdeh, T. J. Overschmidt, K. R. Gaston, *J. Phys. Chem. B 2001*, **105**, *17*, 3663-3674; b) C. S. Sevov, R. E. M. Brooner,

E. Chénard, R. S. Assary, J. S. Moore, J. Rodríguez-López, M. S. Sanford, *J. Am. Chem. Soc.* **2015**, *137*, 14465-14472; c) C. S. Sevov, D. P. Hickey, M. E. Cook, S. G. Robinson, S. Barnett, S. D. Minteer, M. S. Sigman, M. S. Sanford, *J. Am. Chem. Soc.* **2017**, *139*, 2924-2927; d) K. H. Hendriks, C. S. Sevov, M. E. Cook, M. S. Sanford, *ACS Energy Lett.* **2017**, *2*, 2430-2435.

[16] C. S. Sevov, K. H. Hendriks, M. S. Sanford, *J. Phys. Chem. C* **2017**, *121*, 24376-24380.

[17] P. W. Antoni, T. Bruckhoff, M. M. Hansmann, *J. Am. Chem. Soc.* **2019**, *141*, 9701-9711.

[18] H. Hellmann, S. Mooney, *Molecules* **2010**, *15*, 442-459.

[19] https://fi.espacenet.com/publicationDetails/biblio?II=0&ND=3&adjacent=true&locale=fi_FI&FT=D&date=19980616&CC=US&NR=5766894A&KC=A

[20] For the comprehensive overview, see: Y. G. Shtyrlin, A. S. Petukhov, A. D. Strelnik, N. V. Shtyrlin, A. G. Iksanova, M. V. Pugachev, R. S. Pavelyev, M. S. Dzyurkevich, M. R. Garipov, K. V. Balakin, *Russ. Chem. Bull.* **2019**, *68*, 911-945.

[21] For examples of side chain functionalization, see: a) W. Korytnyk, P. Burton, *J. Med. Chem.* **1970**, *13*, 187-191; b) J. A. Yazarians, B. L. Jiménez, G. R. Boyce, *Tetrahedron Lett.* **2017**, *58*, 2258-2260.

[22] For the synthesis of vitamin B_6 derived Schiff base complexes, see: S. Gupta, *Rev. Inorg. Chem.* **2021**, *42*, 161-177.

[23] For the applications of vitamin B_6 in heterocyclic synthesis, see: a) F. Fringuelli, G. Brufola, O. Piermatti, F. Pizzo, *Heterocycles* **1997**, *45*, 1715; b) V. Y. Sosnovskikh, V. Y. Korotaev, A. Y. Barkov, A. A. Sokovnina, M. I. Kodess, *J. Fluor. Chem.* **2012**, *141*, 58-63; c) L. Pizzuti, I. Casadia, T. O. Daher, S. Moura, D. F. Back, E. Faoro, C. S. Schwalm, G. A. Casagrande, G. C. Paveglio, *Synthesis* **2020**, *53*, 365-370.

[24] A. Hamza, F. B. Németh, Á. Madarász, A. Nechaev, P. Pihko, P. Peljo, I. Pápai, *Chem. Eur. J.* **2023**, *29*, e202300996.

[25] M. Chatenet, B. G. Pollet, D. R. Dekel, F. Dionigi, J. Deseure, P. Millet, R. D. Braatz, M. Z. Bazant, M. Eikerling, I. Staffell, P. Balcombe, Y. Shao-Horn, H. Schäfer, *Chem. Soc. Rev.* **2022**, *51*, 4583-4762.

[26] K. M. Pelzer, L. Cheng, L. A. Curtiss, *J. Phys. Chem. C* **2017**, *121*, 237-245.

[27] a) C. Costentin, *Chem. Rev.* **2008**, *108*, 2145-2179 b) R. Tyburski, T. Liu, S. D. Glover, L. Hammarström, *J. Am. Chem. Soc.* **2021**, *143*, 560-576

[28] R. H. Wopschall, I. Shain, *Anal. Chem.* **1967**, *39*, 1514-1527.

[29] F. Wang, S.S. Stahl, *Acc.Chem.Res.* **2020**, *53*, 561-574

[30] J. M. Mayer, *Annu. Rev. Phys. Chem.* **2004**, *55*, 363-390

[31] K. Ando, Y. Shimazu, N. Seki, H. Yamataka, *J. Org. Chem.* **2011**, *76*, 10, 3937-3945.

[32] A. Shrestha, K. H. Hendriks, M. S. Sigman, S. D. Minteer, M.S. Sanford, *Chem.Eur.J.* **2020**, *26*, 5369-5373.

[33] S. Samaroo, C. Hengesbach, C. Bruggeman, N. G. G. Carducci, L. Mtemeri, R. J. Staples, T. Guarr, D. P. Hickey, *Nat. Chem.* **2023**, 15, 1365-1373.